IOPscience iopscience.iop.org

Home Search Collections Journals About Contact us My IOPscience

Solvent-driven polymeric micro beam device

This article has been downloaded from IOPscience. Please scroll down to see the full text article.

2010 J. Micromech. Microeng. 20 085030

(http://iopscience.iop.org/0960-1317/20/8/085030)

View the table of contents for this issue, or go to the journal homepage for more

Download details:
IP Address: 130.126.178.20
The article was downloaded on 05/11/2010 at 03:11

Please note that terms and conditions apply.

J. Micromech. Microeng. **20** (2010) 085030 (7pp) doi:10.1088/0960-1317/20/8/085030

Solvent-driven polymeric micro beam device

Chunguang Xia, Howon Lee and Nicholas Fang

Department of Mechanical Science and Engineering, University of Illinois, 1206 W Green St, Urbana, IL 61801, USA

E-mail: nicfang@illinois.edu

Received 30 March 2010, in final form 21 May 2010
Published 19 July 2010
Online at stacks.iop.org/JMM/20/085030

Abstract

The response of current hydrogel devices mainly depends on the diffusion of stimuli. However, diffusion is a slow transport mechanism compared to advection, which therefore limits the response speed of hydrogel devices. To overcome this limitation, we introduce a capillary network and elastic instability mechanism. Particularly, an open surface capillary delivers and distributes solvent, thus triggering the swelling and bending of curved polymeric beams. To demonstrate this concept, we fabricate these polymeric microstructures using projection micro-stereolithography (PμSL). Combined with instability criteria analysis based on static beam theory, this device is designed to exhibit two-way snap-through behavior. Our analysis provides the minimum dimensionless stiffness β for the beam device to snap during solvent actuation. Here, β is a well-defined dimensionless parameter in our analysis that indicates whether the device can provide sufficient axial force to trigger the snap-through of the beam. The actuation displacement can be as high as 45% of the length of the beam. We observe a maximum midpoint speed of 3.1 cm s^{-1} for a beam 2 mm long—20 times higher than that for a beam without an elastic instability mechanism. This device can be used in artificial muscle and as the key component for fluidic-to-mechanical signal transduction in active micro-fluidic circuits.

(Some figures in this article are in colour only in the electronic version)

1. Introduction

Many applications of hydrogels depend on their unique solvent-swollen properties. Their swelling and shrinking behaviors can be triggered by different stimuli, such as by solvents with different ion concentrations [1], temperature [2], and radiations [3]. The solvent-stimulated swelling phenomenon in hydrogels has long been recognized and investigated theoretically and experimentally [4–6]. The unique characteristics of these polymers have led to some interesting micro devices and applications [7–13]. However, due to fabrication challenges, these gel devices are often formed into simple geometries such as spheres and strips. Moreover, they can only operate in solvents. The response speed is also a great concern for hydrogel devices. It is well known that solvent transport in gels is diffusion dominated. The slow pace of the diffusion process is responsible for the slow responses of hydrogels and further limits the application of polymer swelling in microfluidic devices and other applications, like artificial muscles.

To overcome the diffusion speed limit, we introduced a micro capillary network into a hydrogel device [14]. The capillaries serve as 'highways' for long-range solvent transport by capillary force. In this case, diffusion transport only occurs locally (short range) across the capillary walls. Compared to diffusion, capillary flow is much faster. The velocity of the solvent front in a capillary can be estimated by $T_s\cos(\theta)R/(4\eta L)$ [15], where T_s and η are the surface tension and the viscosity of the solvent, respectively, θ is the contact angle, R is the hydraulic radius of the capillary and L is the length of the solvent in the capillary. Although the solvent front velocity may differ from solvent to solvent, it is clear that, generally, capillary flow is much faster than the diffusion process by several orders of magnitude. Therefore, capillary networks dramatically increase the speed of long-range solvent transport and of the gel response. Nevertheless, the gel response is still dominated by local diffusion. The speed of

 © 2010 IOP Publishing Ltd Printed in the UK & the USA

local solvent transport cannot be increased without applying external driving forces, such as pressure, which increase the operation cost of the gel devices.

As a cheap and effective means to overcome these limitations, we introduce an elastic instability mechanism into polymer gel devices in this work. In this way, the elastic energy during the slow gel swelling or shrinking process is stored in the device and is subsequently released quickly by taking advantage of the elastic instability. As a demonstration, in this paper we focus on micro gel beam structures. Incorporation of stability into silicon micro-electro-mechanical systems (MEMSs) is not a new idea. The simplest mechanical bistable system can be developed by applying an axial compressive force at both ends of a slim beam. If the force exceeds a certain value, the beam buckles into one of two possible stable states [16]. A more general bistable system may incorporate additional transverse forces with different configurations [17–19], thermally introduced compressive force [20] or use the electro-thermal bimorph effect [21]. However, little attention has been given to polymer gel devices, to the best of our knowledge. Although a device with snapping surfaces has been created using poly(dimethyl siloxane) [22], the complicated actuation method is worth further improvement. Polymeric devices have great potential in the development of artificial muscles and as transducers for micro-fluidic circuits (fluidic signals to mechanical power output). In such applications, the available trigger signals are usually solvents or the desired ion concentration; therefore, external transverse force is not preferred for triggering the instability mechanism, nor is the thermal expansion effect. As a solution, we propose the use of locally controlled gel swelling and shrinking to trigger instability. In this case, the only input is the solvent from micro-fluidic circuits and the device can be actuated off-plane. Furthermore, we established the criteria for the beam design by providing the minimum dimensionless stiffness of the beam device and the minimum energy to trigger the snap-through instability. In the following sections, the fabrication and principle of operation of the device are presented in section 2; in section 3 we present a discussion of our design criteria based on elastic static theory. Finally, we present indicators of the device performance.

2. Fabrication and principle of operation

There are several micro fabrication techniques for soft materials [23]. The traditional silicon-based MEMS technology requires expensive industrial instruments and shows limitation in three-dimensional (3D) fabrication. Although the soft lithography and nano-imprint lithography offer nano scale resolution, their advantages are shaded due to the need of physical molds. As a cheap and fast method for polymer gel fabrication, photo-polymerization is the most attractive. However, in order to construct a complicated 3D microstructure, advanced technologies and methodologies need to be incorporated to guide photo-polymerization in 3D space. Here we propose to use a well-established 3D micro fabrication technology, projection micro-stereolithography (PμSL) [24, 25] for 3D soft material fabrication, as highlighted

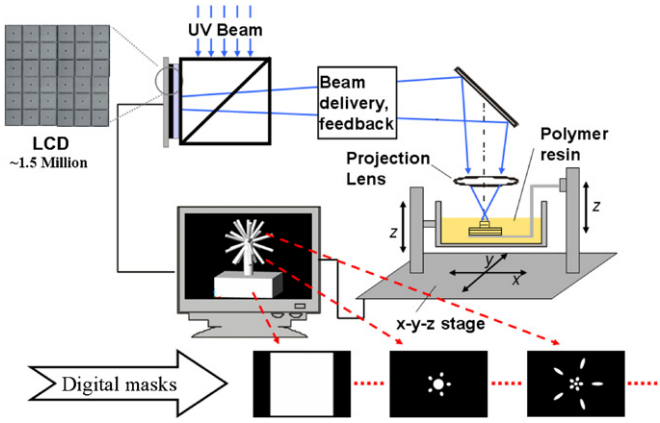

Figure 1. Projection micro-stereolithography system.

in figure 1. The process starts by generating a 3D structure using computer-aided design (CAD) software and then slices the structure into a sequence of mask images (digital mask). Each image represents a thin layer of the 3D structure. During a fabrication cycle, a single image is displayed on the reflective LCD panel. The image on the LCD is then delivered and projected onto the photo curable liquid surface. The whole layer (usually 5–30 μm thick) is polymerized simultaneously. After one layer is solidified, the polymerized component is re-immersed into the resin to allow the formation of a new thin liquid layer on top of it. By repeating the cycle, a 3D microstructure is formed from a stack of layers. The resin monomer used in this work is water-soluble polyethylene glycol (PEG) diacrylate (MW575, Sigma-Aldrich). Bis(2,4,6-trimethylbenzoyl)-phenylphosphineoxide (Irgacure 819, from Ciba) is used as the photoinitiator. We mix 0.75 wt% of light absorber with the PEG monomer to control the UV penetration depth in the solution. The wavelength for the light source is 436 nm and the light intensity is 3.32 mW cm^{-2}.

The designed polymeric device has the shape as shown in figure 2. It consists of three parts: a curved, flat beam (red) with open channels (green) on one of the surfaces; a hollow faucet (blue), which delivers the solvent to the channels and a U-shaped elastic frame (orange), all made of the same PEG material. The overall dimensions of the frame are 3.5 mm $\times$ 2 mm $\times$ 1 mm, and the beam is 175 μm thick with channels that are 90 μm wide and 75 μm deep. One way in which our beam differs from silicon MEMS curved beams, whose curvature is formed from the introduction of an initial residue stress, is that our designed beam is initially curved without appreciable residue stress. Initial residue stress is a costly and hard-to-control process; therefore, our design represents a cheaper and easier alternative for achieving curved beams. Upon solvent delivery to the inlet of the faucet, a strong capillary force drives the solvent through the inner channel of the faucet and dispenses it to the four connected open channels. As observed in the experiment, this happens in a period of less then 20 ms. Compared to the diffusion speed, we can assume that all the channels are filled with solvent at the same time. This assumption is essential for later theoretical analysis. When the PEG contacts the solvent, the wetted gel starts to swell. However, wetting of the whole

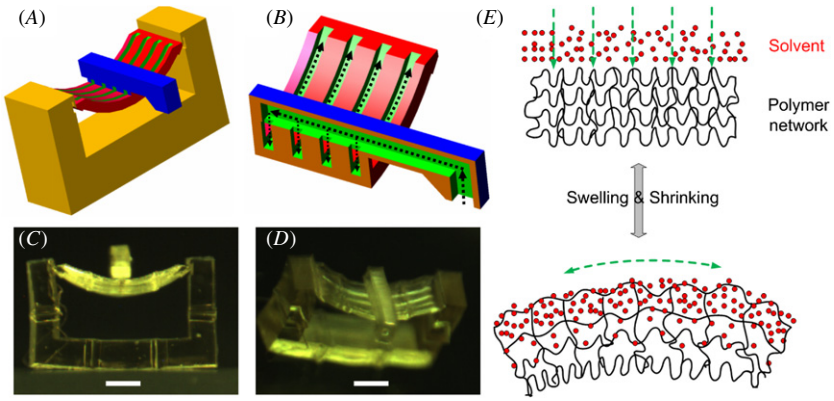

Figure 2. (*A*) The CAD design of the polymer gel bistable device. (*B*) A half section view of the curved beam. The arrows indicate the direction of the solvent flow. (*C*), (*D*) Optical images of the microfabricated sample. Scale bars are 500 μm. (*E*) The mechanism of solvent-introduced bending of hydrogel beams.

curved beam takes longer than the time scale of desired experiments, thus the solvent only wets a portion of the curved beam (figure 2(*E*)). As a result, for a relatively long time, the beam is roughly divided into two layers: a wet layer and a dry layer. The wet layer swells and expands, while the dry layer is stretched. This is similar to the thermal bimorph effect, which also has two distinct material layers. The strong shear stress causes a change of the beam curvature. In our design, the beam curvature decreases and the end-to-end span of the beam increases as the solvent further diffuses into the polymer. However, the dry elastic frame resists the increase of the elongation of the beam by applying a pair of compressive forces at both ends of the curved beam. This causes an increase in the internal elastic energy in the device. As the curvature reaches a critical value, the compressive force generated by the frame may be not sufficient to constrain the beam, causing the beam to snap. Conversely, when the solvent evaporates, the wet part will begin to shrink and reverse the curvature towards its initial shape. It is shown in our analysis and experiment that if the buckling occurs in the swelling process, then the device will experience buckling in the shrinking process as well. In the next section, we develop a simple static theory to explain the mechanism of the buckling and draw criteria for buckling beam design.

3. Design criteria

Euler's column theory states that as a compressive force P acting at the ends of a straight bar exceeds a critical value it will become unstable and buckle. Therefore when a curved beam is subjected to an elastic support and at the same time changes its curvature, the force resulting from the elastic response of the support may exceed this critical value and cause the beam to change curvature abruptly. This mechanism can be integrated into our solvent actuated polymeric beams to dramatically improve the response speed thus increase the transient mechanical power output. In this section we will show the design of a polymeric beam system with elastic instability response.

Let us, for example, consider a simple case in which the interaction between the beam and the support is only

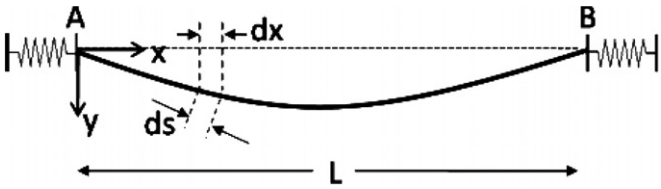

Figure 3. An initially curved beam with elastic supports.

a longitudinal force P, no external bending moment exists (figure 3). We assume the beam has an initial sinusoidal shape as:

$$y_0 = a_n \sin\left(\frac{\pi}{L}x\right). \tag{1}$$

The initial shape is the shape in the absence of external compressive force P and it changes during experiment due to swelling. This initial shape changes as the solvent starts to diffuse into the wall of the capillary which is embedded in the beam, and we further assume that the beam maintains the sinusoidal shape (dominant shape, only the magnitude a_n changes) during this process. To be more precise, from now on we will denote the initial shape as natural shape (shape under no external force) and the associated deflection as natural deflection. Similarly, the shape under external forces will be denoted as actual shape and the associated deflection as actual deflection. In order to focus on the essential mechanisms involved in this process using a simple model, we postpone consideration of developing a full theory for the device; instead, we try to use a simple linear beam theory that does not take into account the compression and extension of the beam (it can be shown that the effects of compression and extension are small [26]). The actual deflection under the lateral load P is derived in [27] and it is given by

$$y = \frac{a_n}{1-\alpha}\sin\left(\frac{\pi x}{L}\right). \tag{2}$$

Here $\alpha = \frac{P}{P_{\mathrm{er}}} = \frac{PL^2}{\pi^2 \mathrm{EI}}$, it is a dimensionless parameter, and EI is the flexural rigidity of the beam. $P_{\mathrm{er}} = \frac{\pi^2 \mathrm{EI}}{L^2}$ is the critical load to make a straight beam with hinged ends for buckling [16]. From equation (2), we find that the actual deflection is

magnified by a factor $\frac{1}{1-\alpha}$, and the actual midpoint deflection is given by setting $x = L/2$:

$$a_a = \frac{a_n}{1-\alpha}. \tag{3}$$

The linear response of the support is taken to be $P = k_s \Delta x$, here Δx is the displacement and k_s is the rigidity of the support. The scenario of the system performance is that as the curvature of the beam changes, the end-to-end span also changes, which is coupled with the elastic response from the support. The change of the end-to-end span of the beam can be calculated by comparing the length difference between the curved beam and the projection of the beam on the x axis. The difference of each pair of corresponding elements is

$$\mathrm{d}s - \mathrm{d}x = \mathrm{d}x\sqrt{1 + \left(\frac{\mathrm{d}y}{\mathrm{d}x}\right)^2} - \mathrm{d}x. \tag{4}$$

Therefore, for small deflection, the displacement of the end of the beam is given by

$$\Delta x = \int_0^{\frac{l}{2}} (\mathrm{d}s - \mathrm{d}x) \approx \frac{1}{2}\int_0^{\frac{l}{2}} \left(\frac{\mathrm{d}y}{\mathrm{d}x}\right)^2 \mathrm{d}x. \tag{5}$$

However the original (fully dry sample) shape of the beam is not a straight one, instead it is sinusoidal shape given by $y_0 = a_0 \sin(kx/L)$. Taking this into account, the displacement of the end during curvature change of the beam is

$$\Delta x = \frac{1}{2}\int_0^{\frac{l}{2}} \left(\frac{\mathrm{d}y_0}{\mathrm{d}x}\right)^2 \mathrm{d}x - \frac{1}{2}\int_0^{\frac{l}{2}} \left(\frac{\mathrm{d}y}{\mathrm{d}x}\right)^2 \mathrm{d}x. \tag{6}$$

Substituting y_0 and equation (2) into this equation gives

$$\Delta x = \frac{\pi^2}{8L\left(a_0^2 - \frac{a_n^2}{(1-\alpha)^2}\right)}. \tag{7}$$

The linear support also provides

$$\Delta x = \frac{p}{k_s}. \tag{8}$$

From equations (7) and (8) we have

$$\tilde{a}_n^2 = (1-\beta\alpha)(1-\alpha)^2 \tag{9}$$

where $\tilde{a}_n = a_n/a_0$ is the dimensionless natural midpoint deflection and

$$\beta = \frac{8\mathrm{EI}}{k_s L a_0^2} \tag{10}$$

is also a dimensionless parameter which is proportional to the ratio of the flexural rigidity of the beam and the rigidity of the support. We can also define the dimensionless actual midpoint deflection from equation (3) by dividing both sides with a_0, then

$$\tilde{a}_a = \frac{a_a}{a_0} = \frac{\tilde{a}_n}{1-\alpha}. \tag{11}$$

Equations (9) and (11) give the parametric relations between the dimensionless natural midpoint deflection and the dimensionless actual midpoint deflection. In equation (9), the left-hand side $\left(\tilde{a}_n^2\right)$ is non-negative and $(1-\alpha)^2$ on the right-hand side is also non-negative; therefore, the following inequality must be satisfied:

$$1 - \beta\alpha \geqslant 0. \tag{12}$$

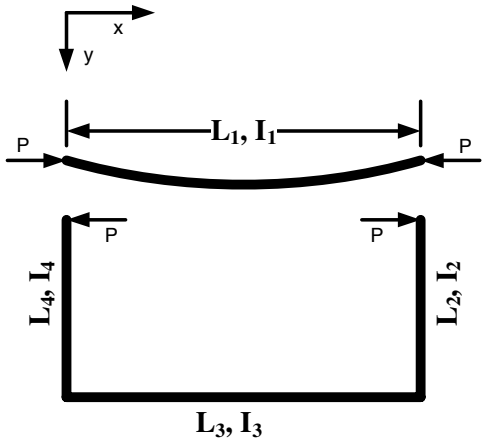

Figure 4. Model for a microgel bistable beam device.

However, Euler's column theory [28] states that the minimum axial force required to cause the buckling of beams with hinged ends is $P_{\mathrm{er}} = \pi^2 \mathrm{EI}/L^2$. We notice that $\alpha = P/P_{\mathrm{er}}$. Therefore, for the beam to snap, α must be $\geqslant 1$, from equation (12), we obtain

$$\beta \leqslant 1. \tag{13}$$

In the device as shown in figure 2, the elastic support is a U-shaped frame. We model the complex geometry of our gel device as four simple beams with the lengths and moments of inertia shown in figure 4. From our experiments, the volume ratio of solvent is less than 5% during most of the time in the actuation. Therefore all beams are assumed to have the same Young's modulus E, and it remains the same during swelling. Beams 2 and 4 are identical, and both are fixed with beam 3. Beam 1 is connected to beams 2 and 4 only by a thin film of 20 μm thickness. Therefore, we model beam 1 as hinged to beams 2 and 4, as the rotation resistance is small. As a result, the interaction between beam 1 and beams 2 and 4 is only a pair of longitudinal P. Therefore, the rigidity of this support has an expression [29]

$$k_s = \frac{6\mathrm{EI}_2 I_3}{3L_2^2 L_3 I_2 + 2L_2^3 I_3}. \tag{14}$$

Substituting this expression into equation (10) we have

$$\beta = \frac{8L_2^2 I_1}{\left(\alpha_0^2 L_1\right)\left(\frac{L_3}{2I_3} + \frac{L_2}{3I_2}\right)}. \tag{15}$$

It can be rewritten as

$$\beta = \frac{P_{\mathrm{er}}\left(\frac{L_2^2 L_3}{2\mathrm{EI}_3} + \frac{L_2^3}{3\mathrm{EI}_2}\right)}{\frac{\pi^2 a_0^2}{8L_1}}. \tag{16}$$

Therefore, β is also the ratio of the end deflection of beam 2 when $P = P_{\mathrm{er}}$ to the extension of beam 1 due to the original deflection y_0 which is the maximum extension. This means that in order for buckling to take place, the resistant force from the support should be larger than P_{er} as the beam reaches the maximum extension. From equation (16), to achieve that, the initial deflection of beam 1 should be large, and the flexural rigidity of beams 2, 3 and 4 needs to be large compared

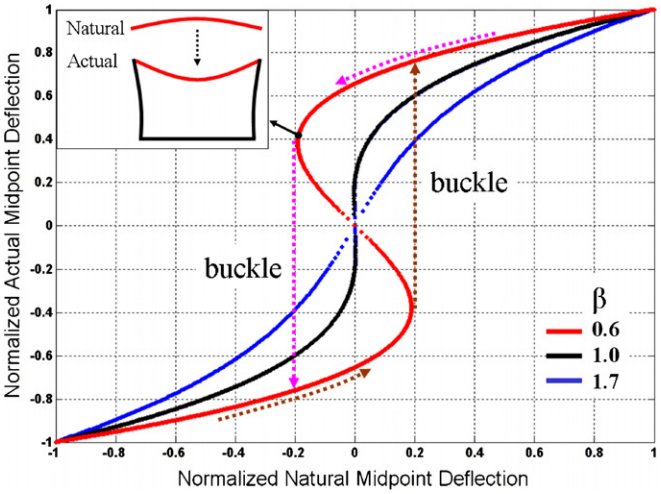

Figure 5. The dependence of the relationship between the actual and the natural midpoint deflection on the geometric parameter β.

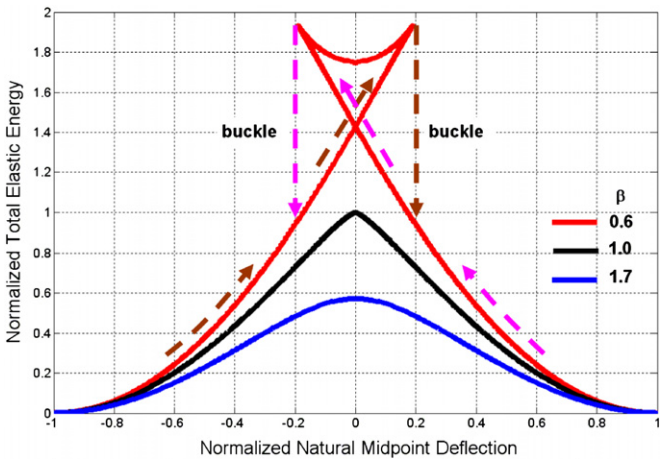

Figure 6. The dependence of the relationship between the total elastic energy and the natural midpoint deflection on the geometric parameter β.

to beam 1 as well. In this way, the U-shaped frame can provide enough axial force to trigger the buckling of curved beams. As can be seen in figure 5, the critical value of β that separates the buckling region ($\beta < 1$) and smooth deformation region ($\beta > 1$) is unity. Polymer swelling or shrinking causes the natural deflection to monotonically decrease or increase, respectively. In the buckling region, during the change in natural deflection, the actual deflection jumps from one side to another at certain points. These points are the unstable configurations in which the buckling occurs. However, when $\beta > 1$, the actual deflection changes continuously with the natural deflection, and no buckling occurs.

It can also be shown that buckling is an energy-favorable phenomenon. Since the compression and extension energies are small [26], the elastic energy is considered to be only bending energy. The bending energy is expressed in the form of [30]

$$U = \frac{1}{2\mathrm{EI}} \int_0^L M^2 \,\mathrm{d}x. \tag{17}$$

Here M is the bending moment. The total elastic energy consists of four portions: the elastic energies stored in beams 1, 2, 3 and 4, with those of beams 2 and 4 being identical. That is,

$$U_{\text{total}} = U_1 + U_2 + U_3 + U_4 = U_1 + 2U_2 + U_3. \tag{18}$$

The bending moment for beams 1, 2 and 4 are

$$\begin{cases} M_1 = P \times y = \frac{Pa_n}{1-\alpha} \sin\left(\frac{\pi}{L_1}x\right) \\ M_2 = P \times x \\ M_3 = P \times L_2. \end{cases} \tag{19}$$

Combining (17)–(19), we have

$$U_{\text{total}} = \frac{P^2 a_n^2 L_1}{4\mathrm{EI}_1(1-\alpha)^2} + \frac{P^2 L_2^3}{3\mathrm{EI}_2} + \frac{P^2 L_2^2 L_3}{2\mathrm{EI}_3}. \tag{20}$$

Dividing both sides of (20) by $U_0 = \frac{P_{\text{er}}\pi^2 a_0^2}{8L_1}$ gives the dimensionless total elastic energy:

$$\tilde{U}_{\text{total}} = (2 + \beta - 2\beta\alpha)\alpha^2. \tag{21}$$

Here $\tilde{U}_{\text{total}} = \frac{U_{\text{total}}}{U_0}$. From the expression of U_0, it can be seen that U_0 is the work done by the critical load P_{er} over the distance equivalent to the shortening of beam 1 (equation (5)) due to the initial deflection y_0. Equations (9) and (21) reveal the relationship between the elastic energy $\tilde{U}_{\text{total}}$ and the natural midpoint deflection $\tilde{a}_n$ of beam 1. As shown in figure 6, in the buckling region ($\beta < 1$), the elastic energy keeps accumulating until snapping takes place. The accumulated elastic energy suddenly drops and mostly transfers into kinetic energy. When $\beta > 1$, the elastic energy changes smoothly with the natural deflection. No sudden drop of energy is observed. The drop in energy increases as β decreases. This can be achieved by increasing the initial deflection of beam 1 or making the flexural rigidities of beams 2, 3 and 4 higher. From (18), when $\beta = 1$, the maximum of $\tilde{U}_{\text{total}}$ is 1 or $U_{\text{total}} = U_0$. Therefore the minimum energy required to trigger the buckling of this curved beam device is U_0. This energy comes from the Gibbs energy change during solvent and polymer mixing or separation (solvent evaporation) [31]. Therefore it is a material property associated with particular polymer–solvent system and thus it also provides a criterion for the material selection during the device design. Unfortunately, solvent transport in polymers is coupled with large deformations and is still a difficult and unsolved problem; further theoretical investigation is needed to understand and predict such phenomena at full scale.

4. Device performance

Using previous static analysis, we designed and fabricated two samples with $\beta = 0.4$ and $\beta = 1.6$ using PμSL. The dimension of the curved beam was the same in both samples, with an end-to-end span of 2 mm, a thickness of 175 μm and channels that were 90 μm wide and 75 μm deep. We changed the value of β by changing the dimensions of the U-shaped frame, in which case we were able to reduce the β value by increasing the thickness of beams 2, 3 and 4. Immediately following the PμSL process, the samples were immersed in acetone and shielded (by covering) from ambient light for 24 h to remove

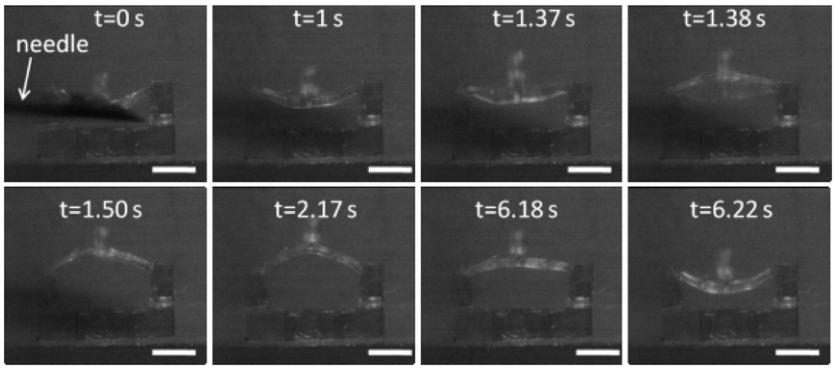

Figure 7. Time frames of the bistable beam device ($\beta = 0.4$) actuated by a drop of acetone. Scale bars are 1 mm.

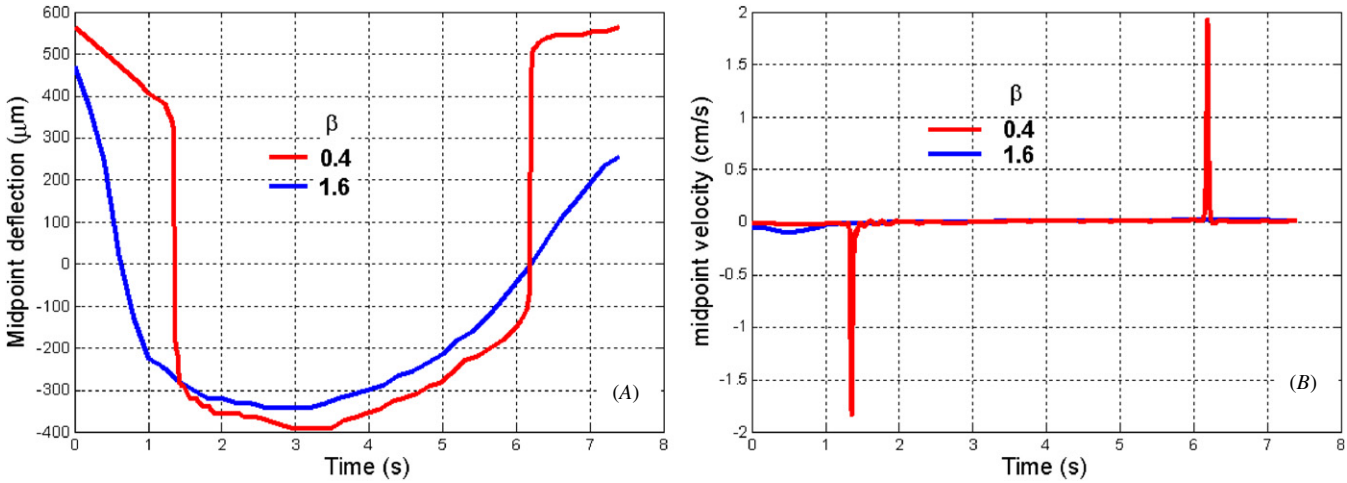

Figure 8. (*A*) Measured midpoint deflection of curve beams during solvent actuation. (*B*) Calculated midpoint velocity during solvent actuation.

residual monomers, preventing further photo-polymerization. The samples were then dried at room temperature for 20 min before 0.5 μL acetone was delivered to them through the inlet of the faucet by a syringe. An acetone droplet was first pushed out and it attached to the needle tip. Then the needle was moved to the faucet, making the droplet touch with the faucet. The droplet was immediately sucked into the faucet and almost at the same time the faucet detached from the needle tip due to disappearance of the droplet and the moving away of the faucet.

A video camera with a frame rate of 60 fps recorded the motion of the beams (figure 7). The videos were analyzed and the mid-point deflection of the beams in both samples was measured (figure 8(*A*)). It is clearly shown that when $\beta < 1$, the beam snaps up and down during polymer swelling and shrinking, respectively. For $\beta = 0.4$, the snap-through instability occurs at 54% of the initial deflection which is comparable to the theoretical prediction of 48%. The actuation displacement is 45% of end-to-end span of the beam. This value is much higher than that of silicon MEMS devices, which is typically less than 5% [21]. In contrast, the mid-point deflection transitions smoothly in the case of $\beta > 1$. From figure 8(*A*) we can also see that at the beginning of solvent actuation, beams with $\beta > 1$ move faster than those with $\beta < 1$. This is because the beam with $\beta < 1$ takes time to accumulate elastic energy before it suddenly snaps. Figure 7(*B*) more clearly demonstrates that by introducing the instability mechanism, the maximum velocity at the mid-point increases by a factor of at least 20. The highest mid-point velocity we have observed is 3.1 cm s^{-1} with a beam length of 2 mm.

The mid-point speed increases as β decreases which requires a stiffer U-shaped frame. However as we mentioned above, the elastic energy stored in the device comes from the mixing energy of the polymer and solvent. This amount of total energy is not changed when we increase the flexural rigidity of the U-shaped frame. Thus, in order for the beam to snap, the mixing energy should be larger than the stored elastic energy when the device is in an instable configuration. However, if the mixing energy is too small to overcome the energy threshold associated with instable configurations, the beam will never snap, even when $\beta < 1$. Therefore, increasing the flexural rigidity of the U-shaped frame can increase the mid-point speed during buckling. But the increase of the flexural rigidity is only up to a critical point, above which further increase will fail to cause the beam to snap. Prediction of the mixing energy during swelling in this device requires further theoretical investigation.

5. Conclusion

In an effort to increase the response speed of a hydrogel device during solvent actuation, in this paper we report on the design, analysis, fabrication and testing of a novel polymeric bistable device. We introduced a capillary network into a hydrogel device in such a way as to dramatically increase the rate of long-range solvent transport (compared with diffusion-based mechanisms), while also providing a means to locally control the swelling of hydrogel. We realized control of surface-oriented swelling in a curved polymeric beam, which also affected its bending direction. Compared with traditional silicon MEMS devices, using this method we achieved much higher actuation displacement with respect to the length of the beam without sacrificing the actuation speed. To further increase the transient response speed, we introduced an elastic instability into our beam design. Combined with a design criteria analysis based on static beam theory, we proved in our experiment the existence of a critical value for the dimensionless parameter β that determines whether or not a curved beam will snap. Further theoretical investigation into solvent transport in polymers coupled with large deformation is needed to fully understand this phenomenon. Due to its unique quick response time, this device has potential for a range of self-powered and autonomous systems, such as microfluidic transducers and valves, artificial muscles and smart drugs.

Acknowledgment

This project was supported by the Gauthier Exploratory Research Foundation.

References

[1] Xu L, Li X, Zhai M, Huang L, Peng J, Li J and Wei G 2007 Ion-specific swelling of poly(styrene sulfonic acid) hydrogel *J. Phys. Chem.* B **111** 3391–7
[2] Ji H, Mourad H, Fried E and Dolbow J E 2006 Kinetics of thermally induced swelling of hydrogels *Int. J. Solids Struct.* **43** 1878–907
[3] Tatsuma T, Takada K and Miyazaki T 2007 UV-light-induced swelling and visible-light-induced shrinking of a TiO_2-containing redox gel *Adv. Mater.* **19** 1249–51
[4] Tanaka T and Fillmore D J 1979 Kinetics of swelling of gels *J. Chem. Phys.* **70** 1214–8
[5] Li Y and Tanaka T 1990 Kinetics of swelling and shrinking of gels *J. Chem. Phys.* **92** 1365–71
[6] De S K, Aluru N R, Johnson B, Crone W C, Beebe D J and Moore J 2002 Equilibrium swelling and kinetics of pH-responsive hydrogels: models, experiments and simulations *J. MEMS* **11** 544–55
[7] Gerlach G, Guenther M, Sorber J, Suchaneck G, Arndt K-F and Richter A 2005 Chemical and pH sensors based on the swelling behavior for hydrogels *Sensors Actuators* B **111–112** 555–61
[8] Herber S, Olthuis W and Bergveld P 2003 A swelling hydrogel-based pCO_2 sensor *Sensors Acutators* B **91** 378–82
[9] Don T-M, Huang M-L, Chiu A-C, Kuo K-H, Chiu W-Y and Chiu L-H 2008 Preparation of thermo-responsive acrylic hydrogels useful for the application in transdermal drug delivery systems *Mater. Chem. Phys.* **107** 266–73
[10] Kim B, Flamme K L and Peppas N A 2003 Dynamic swelling behavior of pH-sensitive anionic hydrogels used for protein delivery *J. Appl. Polym. Sci.* **89** 1606–13
[11] Kim D and Beebe D J 2007 Hydroge-based reconfigurable components for microfluidic devices *Lab Chip* **7** 193–8
[12] Guan J, He H, Hansford D J and Lee L J 2005 Self-folding of three-dimensional hydrogel microstructures *J. Phys. Chem.* B **109** 23134–7
[13] Beebe D J, Moore J S, Bauer J M, Yu Q, Liu R H, Devadoss C and Jo B-Ho 2000 Functional hydrogel structures for autonomous flow control inside microfluidic channels *Nature* **404** 588–90
[14] Xia C, Lee H and Fang N 2008 3D polymeric devices driven by surface micro fluidic capillaries *Proc. ASME Integration and Commercialization of Micro and Nano Systems Int. Conf. and Exhibition*
[15] Washburn E W 1921 The dynamics of capillary flow *Phys. Rev.* **18** 273–83
[16] Timoshenko S P and Gere J M 1961 *Theory of Elastic Stability* (New York: McGraw-Hill) p 76, 77, 84
[17] Vangbo M 1998 An analytical analysis of a compressed bistable buckled beam *Sensors Actuators* **69** 212–6
[18] Taher M and Saif A 2000 On tunable bi-stable MEMS-theory and experiment *J. MEMS* **9** 157–70
[19] Qiu J, Lang J H and Slocum A H 2004 A curved-beam bistable mechanism *J. MEMS* **13** 137–46
[20] Chiao M and Lin L 2000 Self-buckling of micromachined beams under resistive heating *J. MEMS* **9** 146–51
[21] Michael Aron, Kwok Chee Yee, Yu Kevin and Mackenzie Mark R 2008 A novel bistable two-way actuated out-of-plane electrothermal microbridge *J. MEMS* **17** 58–69
[22] Holmes D P and Crosby A J 2007 Snapping surfaces *Adv. Mater.* **19** 3589–93
[23] Quake S R and Scherer A 2000 From micro- to nanofabrication with soft materials *Science* **290** 1536–40
[24] Bertsch A, Zissi S, Jezequel J Y, Corbel S and Andre J C 1997 Microstereophotolithography using a liquid crystal display as dynamic mask-generator *Microsyst. Technol.* **3** 42–7
[25] Beluze L, Bertsch A and Renaud P 1999 Microstereolithography: a new process to build complex 3D objects *Proc. SPIE* **3680** 808–17
[26] Pfluger A 1950 *Stabilitatsprobleme der Elastostatik* (Berlin: Springer)
[27] Timoshenko S P and Gere J M 1961 *Theory of Elastic Stability* (New York: McGraw-Hill) p 31, 32
[28] Timoshenko S P and Gere J M 1961 *Theory of Elastic Stability* (New York: McGraw-Hill) p 49
[29] Xia C 2009 Three dimensional polymeric capillary network: fabrication and applications *PhD Thesis* University of Illinois at Urbana-Champaign chapter 5
[30] Timoshenko S P 1955 *Strength of Materials, Part I* 3rd edn (Princeton, NJ: Van Nostrand) p 306
[31] Hong W, Zhao X, Zhou J and Suo Z 2008 A theory of coupled diffusion and large deformation in polymeric gels *J. Mech. Phys. Solids* **56** 1779–93